JACS
JOURNAL OF THE AMERICAN CHEMICAL SOCIETY

ARTICLE

pubs.acs.org/JACS

Site-Specific Hydration Dynamics in the Nonpolar Core of a Molten Globule by Dynamic Nuclear Polarization of Water

Brandon D. Armstrong,[†,||] Jennifer Choi,[§,#] Carlos López,[⊥] Darryl A. Wesener,[§,▽] Wayne Hubbell,[⊥] Silvia Cavagnero,[*,§] and Songi Han[*,‡]

[†]Department of Physics and [‡]Department of Chemistry and Biochemistry and Materials Research Laboratory, University of California—Santa Barbara, Santa Barbara, California 93106, United States

[§]Department of Chemistry, University of Wisconsin—Madison, Madison, Wisconsin 53706, United States

[⊥]Department of Chemistry and Biochemistry and the Jules Stein Eye Institute, University of California—Los Angeles, Los Angeles, California 90095, United States

Supporting Information

ABSTRACT: Water−protein interactions play a direct role in protein folding. The chain collapse that accompanies protein folding involves extrusion of water from the nonpolar core. For many proteins, including apomyoglobin (apoMb), hydrophobic interactions drive an initial collapse to an intermediate state before folding to the final structure. However, the debate continues as to whether the core of the collapsed intermediate state is hydrated and, if so, what the dynamic nature of this water is. A key challenge is that protein hydration dynamics is significantly heterogeneous, yet suitable experimental techniques for measuring hydration dynamics with site-specificity are lacking. Here, we introduce Overhauser dynamic nuclear polarization at 0.35 T via site-specific nitroxide spin labels as a unique tool to probe internal and surface protein hydration dynamics with site-specific resolution in the molten globular, native, and unfolded protein states. The ^{1}H NMR signal enhancement of water carries information about the local dynamics of the solvent within ∼10 Å of a spin label. EPR is used synergistically to gain insights on local polarity and mobility of the spin-labeled protein. Several buried and solvent-exposed sites of apoMb are examined, each bearing a covalently bound nitroxide spin label. We find that the nonpoloar core of the apoMb molten globule is hydrated with water bearing significant translational dynamics, only 4−6-fold slower than that of bulk water. The hydration dynamics of the native state is heterogeneous, while the acid-unfolded state bears fast-diffusing hydration water. This study provides a high-resolution glimpse at the folding-dependent nature of protein hydration dynamics.

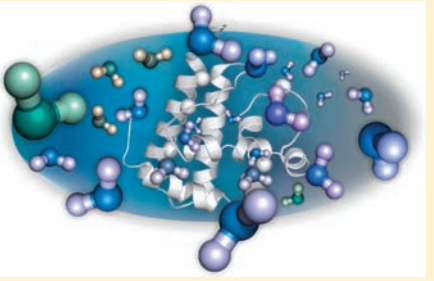

INTRODUCTION

It is appreciated that the hydrophobic effect is one of the dominant forces in protein folding.[1−4] However, the lack of experimental data regarding the location and dynamics of disordered water interacting with proteins, especially in non-native states, has limited a quantitative assessment of the hydrophobic contributions to folding. Many proteins are known to fold via a rapid chain collapse, followed by a slower search for the native state.[5,6] The initial collapsed state is often identifiable as a discrete kinetic intermediate and typically fits the description of a molten globule (MG), i.e., it is compact and highly dynamic and lacks a significant fraction of the native tertiary structure.[7,8] However, whether MG folding intermediates bear a hydrated or dry nonpolar core, and whether any core-associated water is dynamic or spatially confined, are still subjects of debate.[3,9−14] Experimental evidence on the nature of water interacting with the protein core is sorely needed given the fundamental relevance of this problem to the molecular nature of the hydrophobic effect and the role of solvent-mediated internal friction.[15,16] More generally, hydration water—water whose dynamics is perturbed by the protein surface, typically extending up to three water layers—is increasingly recognized to play a direct role in protein dynamics,[17−20] thus regulating protein function, activity and binding events, in addition to folding.[21,22] There is much debate on the time scale, nature, and role of this water,[11,20,23−27] yet experimental reports lag behind theoretical findings or predictions.[3,18,19,28−30] To shed light on these questions, new techniques and experimental studies are needed.

The detection of hydration water poses significant challenges since its spectroscopic signature is largely indistinguishable from the orders of magnitude more populated bulk water. Additionally, the landscape of protein hydration dynamics is heterogeneous on the temporal as well as spatial scale,[18,24−26,29,31,32] requiring tools that can access hydration dynamics within well-defined time scales of interest and with site-specific resolution. Despite the availability of a number of powerful techniques to study the dynamics of macromolecular hydration, including the nuclear Overhauser effect (NOE),[33] ^{17}O, ^{2}H, and ^{1}H nuclear magnetic resonance (NMR) relaxation dispersion,[9,34−37]

Received: December 21, 2010
Published: March 28, 2011

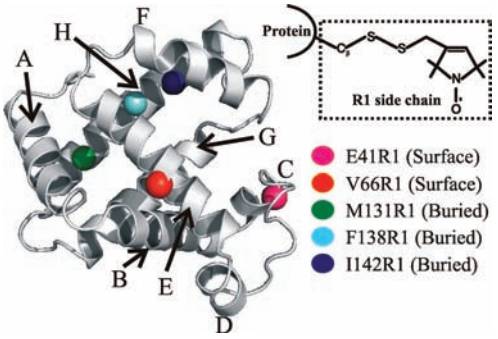

Figure 1. Structure of sperm whale myoglobin (PDB 2mbw;[54] the heme prosthetic group is omitted for clarity). The eight α-helices are labeled, and the five sites analyzed in this work are highlighted. The inset shows the R1 spin label generated via reaction of a methanethiosulfonate reagent with a cysteine side-chain thiol. Image created with PyMOL (version 0.99; DeLano Scientific, San Carlos, CA).

neutron scattering techniques,[20,22,24,32,38−40] terahertz absorption spectroscopy,[41,42] and microwave dielectric spectroscopy,[11] only femtosecond fluorescence spectroscopy[25,26,43,44] on tryptophan and NOE spectroscopic studies on a protein confined inside a reverse micelle[45] have been reported to map out protein hydration dynamics with site-specificity.

This study introduces a novel experimental approach using Overhauser dynamic nuclear polarization (DNP) at 0.35 T to probe the dynamics of hydration water interacting with sperm whale apomyoglobin (apoMb) with site-specific resolution in the molten globule (MG, pH 4), native (N, pH 6.1), and acid-unfolded (U, pH 2.3) states. The Overhauser DNP approach overcomes the above-mentioned challenges by selectively amplifying the ^{1}H NMR signal of water within ∼10 Å of protein residues labeled with nitroxide spin labels.[46] The size of the signal enhancement is sensitive to the timescale modulating the dipolar coupling between the unpaired electron spin and ^{1}H nuclear spin of water.[47,48] Key advantages of this technique over other methods are the unambiguous assignment of the enhanced NMR signal to hydration water, high sensitivity that enables the study of dilute protein solutions (∼100 μM and μL volumes), and the ability to probe core, interfacial, or surface protein sites of interest. Given that the same nitroxide spin label is employed for DNP and electron paramagnetic resonance (EPR), these techniques are used synergistically here, with DNP reporting on hydration dynamics and EPR on protein flexibility and local polarity.

ApoMb offers a unique chance to study the role of hydration water in partially folded species as it populates a stable equilibrium MG intermediate at pH ∼4.1. This species shares a number of key structural features with the apoMb kinetic folding intermediate populated at pH 6, including the MG character.[9,49−52] Several studies have addressed the hydration dynamics of apoMb,[9,11,25,26,53] but only two with site-specific resolution[25,26] and none focused on the buried protein core. Figure 1 illustrates the backbone structure of sperm whale Mb derived from X-ray cyrstallography[54] and the sites chosen for site-directed spin labeling (SDSL) with the nitroxide spin label R1 (inset Figure 1) through a cysteine point mutation.[55] The three sites buried from the solvent, M131, F138, and I142, belong to the H-helix and participate in the ABGH structural core populated in both the kinetic and equilibrium folding intermediates.[49,56,57] In addition, M131 is among the most protected sites from hydrogen/deuterium exchange[58,59] in the N state and is known to be involved in nonspecific nonpolar interactions in the equilibrium MG.[60] Two surface sites, E41 (C-helix) and V66 (E-helix), were chosen as probes of the protein exterior.

Our study finds that the hydration dynamics of native apoMb is very heterogeneous, with the solvent-exposed sites displaying fast water dynamics and the interior sites behaving as a dry core. In contrast, the equilibrium MG has a wet core lubricated with hydration water whose dynamics is intermediate between that of the native and acid-unfolded states.

MATERIALS AND METHODS

Protein Expression, Purification, and Characterization. A modified pET-17b vector (Novagen, Madison, WI) carrying the gene for wild-type sperm whale myoglobin was a generous gift from Steven Boxer (Stanford University, CA). Five mutagenic plasmid DNAs, each carrying one of the apoMb cysteine point mutations E41C, V66C, M131C, F138C, and I142C, were generated via the QuickChange kit (Stratagene, La Jolla, CA), as previously described.[55] Each plasmid was transformed into *E. coli* BL21 DE3 cells (Novagen). *In vivo* protein expression was carried out in LB medium at 37 and 42 °C. ApoMb overexpression was induced upon addition of isopropyl-β-D-thiogalactopyranoside (1 mM) at OD_{600} = 0.8. Cells were harvested at $OD_{600} \approx 1.8$. Cell lysis, inclusion body resuspension, and HPLC purification were performed according to published procedures.[61,62] Protein purity and identity were assessed by reverse-phase analytical HPLC and either electrospray ionization or MALDI mass spectrometry.

Generation of Nitroxide-Labeled ApoMb. Lyophilized apoMb was solubilized in 6 M urea and 10 mM sodium acetate at pH 6.1 for 30 min at 4 °C. For mutants carrying surface Cys (E41C and V66C), the solubilized protein was diluted 7-fold in 10 mM sodium acetate at pH 6.1. A 10-fold molar excess of 1-oxyl-2,2,5,5-tetramethyl-Δ3-pyrroline-3-methyl methanethiosulfonate (MTSL; Toronto Research Chemicals, North York, Ontario, Canada) was added under gentle stirring at 4 °C. For mutants carrying buried Cys (M131C, F138C, and I142C), the solubilized protein was diluted 2.1-fold with 10 mM sodium acetate at pH 6.1 to a final 2.8 M urea concentration before rapid addition of a 10-fold molar excess of MTSL under stirring at 4 °C. Both reactions were allowed to proceed for 18 h at 4 °C. The reaction mixture for the mutants carrying the buried Cys was diluted 3.3-fold with 10 mM sodium acetate at pH 6.1 and incubated for 30 min at 4 °C under gentle stirring, to promote refolding. After the above treatment, each protein solution was dialyzed extensively against 10 mM sodium acetate at pH 6.1 at 4 °C to eliminate urea and excess MTSL. Spin-labeled protein solutions were concentrated with an Amicon Ultra device (3000 MWCO; Millipore, Billerica, MA) and flash-frozen in separate aliquots. Protein concentrations were assessed by absorption spectroscopy (ε_{280} = 15 200 cm^{-1} M^{-1}). Labeling efficiencies were assessed by reverse-phase analytical HPLC on a C_{18} column (Grace, Deerfield, IL). Labeling efficiencies for the DNP and CD samples were as follows: E41R1 and V66R1 >95%; M131R1, F138R1, and I142R1 61−90%. Successful apoMb spin labeling was confirmed by electrospray ionization or MALDI mass spectrometry and electron spin resonance.

Far-UV Circular Dichroism (CD). Far-UV CD experiments were carried out at equilibrium on 10−15 μM protein samples. Data were collected with a MOS-450 spectropolarimeter (Bio-Logic Science Instruments, Claix, France). Quartz cuvettes with 1 and 10 mm path length (Hellma, Müllheim, Germany) were used for spectral scans and titrations at fixed wavelength, respectively. CD scans were performed at room temperature in 1 nm steps, with 20 s signal averaging per step. Mean residue ellipticity (MRE; deg cm^2 $dmol^{-1}$) was determined

according to the relation MRE = $\theta/(10CN_Al)$, where θ denotes the experimental ellipticity (in mdeg), C is the molar concentration of the protein, N_A is the number of amino acids (153 for apoMb), and l is the cuvette path length (in cm). To verify the formation of N, U, and the pH 4.1 intermediate, all nitroxide-labeled samples were subject to equilibrium pH titrations, monitored by far-UV CD at 222 nm. The far-UV CD titrations were carried out at room temperature, and data were signal-averaged for 20 s. A concentrated protein stock solution (ca. 300 μM in 10 mM sodium acetate, pH 6.1) was diluted into 1 mM sodium acetate at pH 6.1 to generate ca. 20 μM protein solutions. The pH of these starting solutions was progressively lowered upon addition of either 0.1 or 1 M acetic acid (to pH ca. 3) or concentrated HCl (to pH < 3). Samples were allowed to equilibrate at the desired pH for ≥10 min prior to data acquisition, and data were collected in sequence on the same sample. Independent duplicate pH titrations were performed on each apoMb variant.

DNP and EPR Measurements. Prior to DNP experiments, samples at the desired pH were eluted through a 2 mL Sephadex G-25 (fine grade, SIGMA) spin column to remove any heavily aggregated species.[51] The column was equilibrated by repeated washes with buffer adjusted to the desired pH. Protein concentrations were assessed by electronic absorption (280 nm) after spin column treatment. Typical concentrations were ~200 μM. DNP experiments were performed at 0.35 T in a Bruker TE_{102} rectangular cavity using a home-built NMR probe and a Bruker Avance 300 NMR spectrometer. Experiments were performed at room temperature while air was continuously flowed through the cavity to minimize sample heating. About 3 μL of sample was loaded into a 0.64 mm i.d. quartz capillary to minimize the electric field at the sample. Further details of our DNP hardware[63] and data analysis[48,64] have been previously described.

EPR spectra were recorded at 22 °C in a Bruker ELEXSYS 580 with a high-sensitivity resonator using an incident microwave power of 20 mW and modulation amplitude of 1 G. Samples of at least 6 μL were loaded in sealed capillary tubes (0.6 mm i.d. × 0.84 mm o.d.; VitroCom, Inc., NJ). Spectra were recorded at X-band frequency with a scan width of 100 G in 25% (w/w) Ficoll 70 to increase the solution viscosity, thereby minimizing the contribution of protein rotational diffusion to the EPR spectral lineshapes. At this concentration, Ficoll has no effect on the internal motion of the R1 spin-labeled side chains.[55] The final protein concentration of the EPR samples was ~200−400 μM. To obtain hyperfine splittings ($2A_{zz}'$) in the absence of motion, EPR spectra were also recorded at −50 °C using an incident microwave power of 0.2 mW and modulation amplitude of 2 G. The hyperfine splittings were determined by individually fitting of the low- and high-field resonances to a mixture of Lorentzian and Gaussian line shapes using the Xepr program (Bruker, Germany) and by measuring the magnetic field separation between the low- and high-field resonances to obtain $2A_{zz}'$. EPR simulations of room-temperature data are described in the Supporting Information.

Overhauser DNP Theory. We provide a brief discussion of the relevant theory, as detailed reports can be found elsewhere.[47,48,64,65] Overhauser DNP is a motion-mediated transfer of electron spin polarization to nuclear spin polarization via dipolar or scalar coupling. Upon steady-state irradiation at the electron spin resonance frequency, the ^{1}H NMR water signal enhancement, E, is given by[47]

$$E = 1 - \rho f s |\gamma_S|/\gamma_I \quad (1)$$

where ρ is the coupling factor, f is the leakage factor, s is the saturation factor describing the extent to which the electron spin population has been driven from equilibrium by microwave irradiation, and γ_S and γ_I are electron and proton gyromagnetic ratios ($\gamma_S/\gamma_I \approx 660$ for an unpaired electron spin and the ^{1}H nucleus). Both ρ and f depend on the rates of nuclear spin transitions caused by the dipolar coupling to the electron spins and are functions of magnetic field and the time scale modulating the dipolar coupling between the two spins. The leakage factor is determined from ^{1}H T_1 relaxation measurements: $f = 1 - T_1/T_{10}$, where T_1 (T_{10}) is the ^{1}H spin relaxation time with (without) the spin label present.[66] The leakage factor is close to 1 if most ^{1}H relaxation occurs via coupling to the unpaired electron. The saturation factor depends on the microwave power and the amount of hyperfine mixing caused by the coupling to the ^{14}N nuclei.[64] For the tumbling times of spin-labeled apoMb, we can approximate s at infinite microwave power to be close to 1.[64] By measuring E as a function of applied microwave power and extrapolating to infinite power, we determine E_{max} for $s = 1$ and can solve eq 1 for ρ. Determining the time scale of the interaction from ρ depends on the model employed to describe the diffusion of the two spins. Unlike in NOE, the electron−nucleus dipolar interaction responsible for DNP is bimolecular, and the ^{1}H-electron coupling is predominantly modulated by translational diffusion. The force-free, hard-sphere (FFHS) translational diffusion model[67,68] has previously been shown to fit NMR dispersion data reasonably well for water interacting with nitroxide radicals in solution,[48,69] water attached to spin-labeled vesicles,[34] and the solvent-exposed sites of a spin-labeled protein.[70] This model is attractive as ρ depends only on the magnetic field and the translational correlation time, τ (assuming the electron spin relaxation times are long compared to τ), through the spectral density function, $j(\omega,\tau)$:

$$\rho = \frac{6j(\omega_S - \omega_I, \tau) - j(\omega_S + \omega_I, \tau)}{6j(\omega_S - \omega_I, \tau) + 3j(\omega_I, \tau) + j(\omega_S + \omega_I, \tau)} \quad (2)$$

$$j(\omega,\tau) = 1 + \frac{\frac{5\sqrt{2}}{8}(\omega\tau)^{1/2} + \frac{\omega\tau}{4}}{1 + (2\omega\tau)^{1/2} + \omega\tau + \frac{\sqrt{2}}{3}(\omega\tau)^{3/2} + \frac{16}{81}(\omega\tau)^2 + \frac{4\sqrt{2}}{81}(\omega\tau)^{5/2} + \frac{(\omega\tau)^3}{81}} \quad (3)$$

where

$$\tau = d^2/(D_I + D_S), \quad (4)$$

ω_S and ω_I are the electron spin and ^{1}H nuclear spin Larmor frequencies, d is the distance of closest approach between the two spins, and D_I and D_s are the translational diffusion coefficients of the ^{1}H of water and the electron spin, respectively. Using eqs 1−4 the translational correlation time of water can be determined from DNP measurements. Recent work has applied more sophisticated techniques to model the coupling and saturation factors.[71−73] Regardless of the dynamic model used, however, ρ decreases as the timescales modulating the electron−^{1}H nucleus dipolar coupling increase, allowing qualitative conclusions to be drawn by comparing ρ values, making DNP a general method for gaining information on hydration dynamics. Although the ^{1}H NMR signal of bulk water is measured, the signal enhancement is heavily weighted toward water within 10 Å of the electron spin due to the strong distance dependence of the dipolar coupling and to the large gyromagentic ratio of the electron spin that makes it the dominant relaxation source.[46] The DNP approach has the further advantage of being able to measure a leakage factor to account for ^{1}H spin relaxation not due to the electron spin. This is in contrast with the intermolecular ^{1}H NOE experiment, where long-range dipolar couplings cannot be neglected.[46]

RESULTS AND DISCUSSION

Effect of Spin Label on ApoMb Structure. Introduction of the R1 spin label at the five sites of apoMb studied here does not have a significant effect on the secondary structure of the native protein, except for a small decrease in helicity observed for F138R1, as shown by the far-UV CD data in Figure 2. Additionally, R1 at buried sites did not cause local unfolding, as evidenced

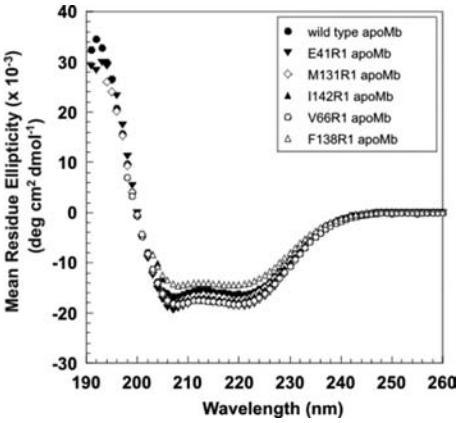

Figure 2. Far-UV circular dichroism spectra of wild-type (●) and nitroxide-labeled (▼, ◇, ▲, ○, △) apoMb variants collected at room temperature. The spectra are averages of three independent experiments.

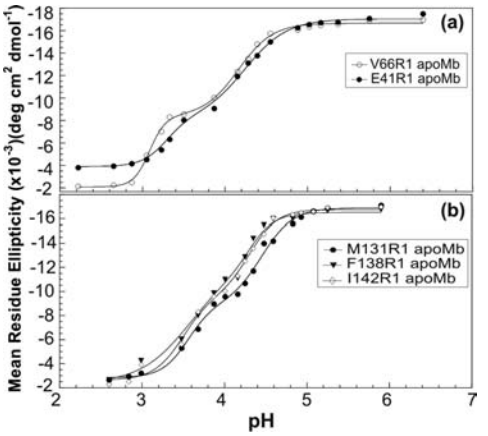

Figure 3. Equilibrium pH titrations of (a) V66R1 (○) and E41R1 (●) and (b) M131R1 (●), F138R1 (▼), and I142R1 (◇) apoMb variants followed by far-UV CD at 222 nm at room temperature. To guide the eye, the experimental data were fit to a model based on a linear combination of Henderson−Hasselbalch equations where we assumed, for simplicity, that each of the two main phase transitions results from the collective protonation/deprotonation of the pertinent residues with ionizable side chains.

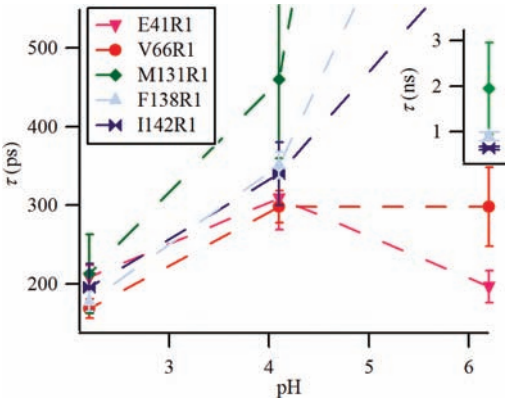

Figure 4. τ for the N (pH 6.1), MG (pH 4.1), and U states (pH 2.2) for the different mutants. The FFHS model was used to estimate τ from ρ. The standard deviation of independent measurements of ρ was used to estimate the error bars. Note that the inset has a different vertical scale. Lines are to help guide the eye.

by the immobilization of the nitroxide, characteristic of R1 in folded structures[74] (see EPR results discussed below). At the tertiary fold level, small-to-large substitutions in the core of the protein, such as the ones made here, may overpack the core and potentially introduce unfavorable steric contacts, unfavorable interactions, and torsional strain.[75] Earlier studies[75,76] showed that the extent of such destabilizing effects depends on the native packing and the internal flexibility of the residue introduced. For example, high-resolution structures of several proteins bearing a small-to-large substitution in the interior, including introduction of an R1 spin label,[74] revealed that the larger side chain can be accommodated by a small shift in the backbone atoms and adjustments of side-chain rotamers without major structural rearrangements.[75,77,78] In fact, substitution of the native residue F138 with a tryptophan in myoglobin had little effect on the tertiary fold of the holo-protein (rmsd = 0.19 Å).[79] Thus, it is likely that introduction of the R1 side chain at apoMb buried sites does not have a substantial effect on the three-dimensional structure of the protein, though small rearrangements of side chains and small shifts of the backbone may be present. In flexible structures such as U or MG states of apoMb, the R1 residue should be accommodated with little energy cost.

The pH titrations shown in Figure 3 reveal that all species populate an equilibrium folding intermediate and that the pH dependence of apoMb equilibrium unfolding is largely preserved in the mutants. Further, previous molecular dynamics simulations with freely dissolved nitroxide radicals[80] and bulk water diffusion measurements from DNP with nitroxide radicals[81] showed that the hydration dynamics determined from DNP is unaffected by the presence of the spin label.

The Nonpolar Core of Native ApoMb. ^{1}H DNP and T_1 measurements of water were used to determine the DNP leakage and coupling factors and to estimate the timescale of diffusion dynamics, τ, of hydration water that is interacting with the nitroxide spin probe (eqs 1−4). The results are shown in Figure 4 and Table 1. Clear differences in ρ (Table 1), and thus τ, are observed between the interior and exterior sites, as well as between the unfolded, equilibrium molten globule, and native states, particularly at interior sites. In the N state, all sites in the nonpolar core display much slower water dynamics than the solvent-exposed sites. Among the interior sites, M131R1 displays the slowest water dynamics (i.e., large τ), followed by F138R1 and I142R1. Large τ values are due to a large distance of closest approach, d, between the radical's electron spin and ^{1}H nuclear spin of water and/or a small translational diffusion coefficient of water near the radical, D_I (eq 4). In either case, given that a decrease in ρ correlates with slower solvent dynamics with respect to the spin label regardless of the model chosen to describe the dynamics of the system,[47] it is clear that the interactions of water with the nonpolar core occur on a much slower time scale than those with the solvent-exposed sites.

Leakage factors are also shown in Table 1 and provide important additional insights. A large τ accompanied by a small f is compatible with the presence of distant water (large d), while a large τ accompanied by a high f for samples with comparable spin label concentration is consistent with slower diffusion of nearby water (small D_I). These are general trends regardless of the dynamic model used; however, alternative interpretations are possible. Here, EPR analysis is crucial to narrow the interpretation

dx.doi.org/10.1021/ja111515s |J. Am. Chem. Soc. 2011, 133, 5987–5995

Table 1. Summary of DNP and EPR Parameters[a]

sample	f	$\rho \times 10^{-2}$	τ (ps)	E_{max}	A_{zz}' (G)	%i	%m
M131R1-N	0.78	0.24 ± 0.2	1950 ± 1000	$+0.2 \pm 1$	34.90	95	5
F138R1-N	0.16	0.9 ± 0.1	908 ± 70	-0.1 ± 0.1	34.38	95	5
I142R1-N	0.36	1.6 ± 0.1	642 ± 25	-2.9 ± 0.1	35.40	61	39
E41R1-N	0.22	8.9 ± 1	197 ± 20	-12 ± 2	36.40	58	42
V66R1-N	0.12	5.2 ± 1	298 ± 50	-3.2 ± 0.9	36.22		100
M131R1-MG	0.383	2.7 ± 0.9	460 ± 100	-6.0 ± 2	35.10	60	40
F138R1-MG	0.13	4.1 ± 0.3	351 ± 15	-2.5 ± 0.2	35.38	59	41
I142R1-MG	0.27	4.3 ± 0.7	340 ± 22	-6.8 ± 1	35.40	60	40
E41R1-MG	0.34	4.9 ± 0.9	309 ± 40	-8.7 ± 0.6	35.74	57	43
V66R1-MG	0.16	5.2 ± 0.4	298 ± 20	-4.4 ± 0.4	36.13	72	28
M131R1-U	0.24	8.1 ± 2	213 ± 50	-12 ± 3			
F138R1-U	0.11	10.1 ± 0.7	178 ± 12	-6.1 ± 0.5			
I142R1-U	0.21	9 ± 2	196 ± 30	-11 ± 2			
E41R1-U	0.18	8.3 ± 0.7	209 ± 15	-8.4 ± 0.5			
V66R1-U	0.12	10.7 ± 0.6	169 ± 12	-7.7 ± 0.4			

[a] Sample concentrations are ~200 μM. E_{max} is the extrapolated DNP signal at infinite microwave power (Materials and Methods). Error in f is ~3−5%. The percentages of immobile (%i) and mobile (%m) components in the EPR spectra were obtained from spectral simulations. Additional parameters obtained from simulations are provided in Table S1.

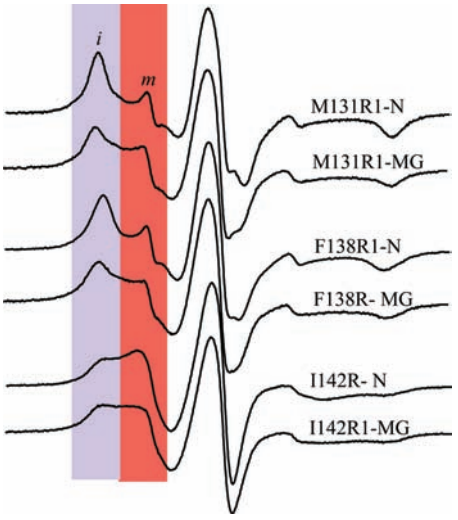

Figure 5. EPR spectra of R1 at the buried sites. Regions shaded in blue and red identify relatively immobile (i) and mobile (m) states, respectively. The m population of M131R1 and F138R1 in the N state is ~5% (Table S1) and likely arises from a small amount of free spin label or unfolded protein. This amount is negligible for DNP so we only consider the i component in the discussion of the N state. In the MG states of M131R1 and F138R1, the m component is ~40% and contributes significantly to the DNP experiments. For I142R1, both i and m components are important in the N and MG states.

and further validate the DNP results as discussed below. The value of f for F138R1 in the N state is smaller than that observed for the other interior sites; hence, we interpret the large τ for this residue as due to remote water on the protein surface and not slowly diffusing water proximal to the spin label. This conclusion is supported by the EPR results discussed below. Residues M131R1 and I142R1 have both large f and τ, suggesting the presence of dynamic water closer to the spin label compared to F138R1. However, EPR analysis was necessary to conclusively assess the origin of the large τ for these two residues.

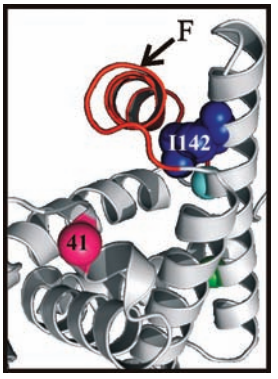

Figure 6. Ribbon diagram of myoglobin showing the position of the native isoleucine 142 in the holo-protein (PDB 2mbw). The heme prosthetic group was omitted for clarity. The region corresponding to the F-helix is highlighted.

The N state EPR spectra of M131R1 and F138R1 reporting on the dynamics of the R1 side chain are shown in Figure 5. The spectral line shapes are characteristic of a nitroxide with restricted motion and tight packing around the side chain. EPR data on frozen samples (−50 °C) were also collected to determine the effective hyperfine splitting, A_{zz}', as this parameter is sensitive to local polarity[82−84] (Table 1; Figure S1). For example, a free nitroxide spin label has A_{zz}' values of 36.88 G in water and 33.78 G in toluene.[84] The A_{zz}' values for residues M131R1 and F138R1 in the N state are close to the value for a free nitroxide in toluene, clearly implying a nonpolar environment around the spin label. These EPR results point to the existence of a "dry" hydrophobic core in the N state, suggesting that the small but measurable DNP effect arises from water located remote from the spin-labeled core (i.e., larger d compared to surface sites). Given this conclusion, the significantly larger f for M131R1 compared to F138R1 suggests the interesting possibility of dynamically restricted bound water closer to M131R1 than F138R1, since distances to rapidly diffusing surface water cannot explain the large observed difference in f. A few bound water molecules (surface or internal) rotating with

dx.doi.org/10.1021/ja111515s |J. Am. Chem. Soc. 2011, 133, 5987–5995

the global protein motion can contribute significantly to electron spin-mediated ^{1}H nuclear spin relaxation rates.[37,85] This extra relaxation competes with the DNP effect, lowering ρ and increasing f. As this effect falls off as $1/r^6$, bound water molecules closer to M131R1 would explain the much larger f than F138R1, consistent with our results that both sites are still "dry".

Among the buried sites in the N state, I142R1 has the smallest τ and largest A_{zz}' values and displays a multicomponent EPR spectrum (Table 1; Figure 5). As shown in Figure 6, I142 is packed against the F-helix in the holo-protein. Both NMR and EPR studies have shown that the F helix in the N state undergoes conformational exchange resulting from removal of the heme in the apo-protein.[55,57,86] Thus, it is likely that the two-component EPR spectrum arises from changes in packing and solvent exposure around I142R1 due to the conformationally fluctuating F helix. Taken together with the DNP data, this observation implies that I142R1 is partially exposed to hydration water possessing a slow apparent diffusion coefficient.

In summary, the small ρ, f, and A_{zz}' values of F138R1 imply that this residue is "dry" in the native state, with the small DNP effect arising from water on the protein surface. M131R1 also displays a small ρ and A_{zz}', implying that this residue is "dry" as well. The large leakage factor arises from significant ^{1}H relaxation by the unpaired electron, which we suggest is due to nearby bound water. In contrast, I142R1 displays ρ, f, and A_{zz}' values consistent with the presence of slowly diffusing water interacting directly with this residue. Therefore, I142R1 is partially hydrated in the native state of the protein, consistent with the less structured environment of this residue in the apo form of the protein.

The MG Core. As shown in Figure 4 and Table 1, the core of the MG state interacts with water and displays significantly faster translational dynamics than the N state, with $\tau \approx 350-450$ ps. This is only a 2-fold retardation compared to the hydration dynamics around the same residues in the U state. The decrease in τ for these sites is accompanied by a decrease in f in the MG relative to the N state (except for F138R1, where f remains relatively constant), implying that the observed DNP effects result from faster diffusing local water compared to the core of the N state. This result suggests that the core of the MG state interacts directly with dynamic water, unlike the core of the N state.

The EPR spectra of all mutants studied here in the MG state display two spectral components that could arise from either different rotamers of R1 or distinct protein conformations.[55] Given that high-resolution NMR studies of the MG state show conformational exchange extended over several regions of the protein, the latter possibility is likely.[50,57] The EPR data further show that the M131R1 and F138R1 side chains are more mobile in the MG compared to the N state, suggesting reduced side-chain packing in the MG core. The higher A_{zz}' value for F138R1 also indicates that this side chain experiences a more polar environment in the MG than in the N state, consistent with the DNP results, which imply the presence of dynamic water in the MG core. In contrast, the MG-state EPR spectrum of I142R1 reflects an overall reduction in mobility of the side chain relative to the N state, as seen by the decrease in the intensity of the more mobile component in Figure 5 and by spectral simulations (Figure S2; Table S1). However, the DNP τ and f values are still significantly smaller in the MG state, implying faster water dynamics near I142R1 in the MG compared to the N state. This result shows that trends of water dynamics around the R1 side chain are not always correlated with side-chain mobility. Last, it is important to note that the estimated τ of 350−450 ps represents a weighted average between the exchanging conformations sampled by the MG. From both the DNP and EPR results, we conclude that the core of the apoMb MG is hydrated with dynamic water. This finding does not necessarily imply that there is much water in the MG core. In fact, the relatively low A_{zz}' values (e.g., compared to the exterior sites, see Table 1) suggest that there may be only a few, yet dynamic, water molecules interacting with the core of the MG.

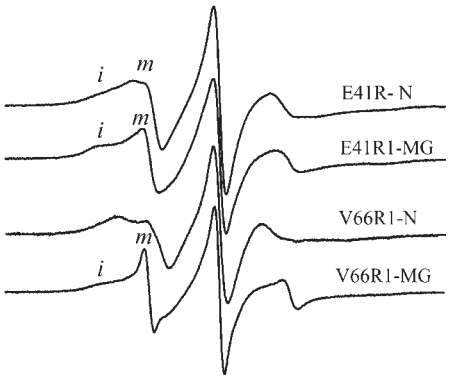

Figure 7. EPR spectra of E41R1 and V66R1 in the N and MG states. *i* and *m* identify components corresponding to relatively immobile and mobile states of R1. Note that V66R1 in the N state displays only one component (see text).

The N and MG Solvent-Exposed Surface. The large differences in τ observed between the buried and solvent-exposed sites (E41R1 and V66R1) in the folded state confirm that water is able to more freely diffuse at the protein surface. At the same time, the observation of heterogeneous surface hydration dynamics, especially in the N state, emphasizes the importance of employing site-specific probes, as charge, polarity, local structural, and chemical topology may all contribute to distinct variations in local water dynamics.[24,31,32] The τ values of 190 and 300 ps for E41R1 and V66R1, respectively, are about 2−4 times slower than the measured τ value of bulk water,[48,87] in agreement with previous results that surface hydration water is slowed by a factor of 2−5 compared to bulk water.[20,32,37,81] The EPR spectra for both surface sites reflect higher mobility of the nitroxide side chain compared to the buried sites, as expected (Figure 7). E41R1 in the N state displays a two-component EPR spectrum, with a relatively immobile component and a mobile component that has a line shape consistent with weakly ordered anisotropic motion characteristic of R1 at helix surface sites.[88,89] Spectral simulations confirm this qualitative description and provide quantitative values for rates and order of motion (Figure S2; Table S1).

In the MG state, E41R1 also displays two EPR spectral components distinct from those of the N state. In particular, a more strongly immobilized component appears, while the more mobile component has lower order (Figure 7; Figure S3; Table S1). The A_{zz}' value of E41R1 is also lower than in N, suggesting that this site has reduced polarity in the MG. A dramatic increase in τ and f is also observed for E41R1 in the MG state compared to the N state. From the DNP and EPR results, we propose that the MG samples non-native conformations in which E41R1 is partially buried. This finding is interesting because non-native conformations of intermediates were suggested to be important

in protein folding.[90,91] A previous study by time-resolved Trp fluorescence also mapped out hydration dynamics around E41, but found faster hydration dynamics in the MG compared to the N state for this residue.[26] This study, however, also found that the hydration dynamics of E41 was similar to that of more buried sites in the N state—a trend not observed by DNP nor generally expected. As mentioned for the MG interior sites, the DNP results report on hydration dynamics averaged over exchanging conformations. It is possible that tryptophan fluorescence spectroscopy is not equally sensitive to conformations with distinctly different exposure to water, which may explain the conflicting observations.

The EPR spectrum of V66R1 in the N state reflects a single dynamic component with ordered anisotropic motion[88] (Figure 7; Figure S3; Table S1). In the MG, the EPR spectrum is quite different from the N state and displays two components, likely caused by conformational exchange in the E helix as previously reported.[57] However, the DNP results show similarly high hydration dynamics between the MG and N states, and the local polarity measured through the A_{zz}' values for V66R1 are similarly high for both the N and MG states. Although the EPR spectrum of V66R1 reveals differences between the local protein motions of N and MG, the DNP results suggest similarly high hydration dynamics for this site in both states.

The Acid Unfolded State. In the U state, all residues display significant solvent exposure, with τ between 169 and 219 ps. The dispersion in τ is much smaller than observed in the MG and N states, though small differences remain (Figure 4; Table 1). The dramatic decrease in the dispersion of τ points to the presence of a highly dynamic and largely unstructured U state, consistent with prior findings.[57,92] This result suggests that the local topology, charge, hydrophobicity, and polarity upon formation of the native tertiary structure are stronger determinants of local hydration dynamics than the primary structure alone.

CONCLUSIONS

Using dynamic nuclear polarization and electron paramagnetic resonance of site-specifically spin-labeled proteins, we were able to probe the diffusion dynamics of hydration water interacting with the surface and interior sites of apoMb. In the native state, all residues studied here have distinctly different hydration dynamics. Specifically, the surface sites (E41R1 and V66R1) display a relatively fast hydration dynamics that is only 2−4 times slower than that of bulk water. In contrast, the DNP and EPR data of M131R1 and F138 confirm the existence of a "dry" interior in the native state. Unlike M131R1 and F138R1, the core residue I142R1 interacts directly with dynamic water, likely due to the disordered F-helix of the apo-protein, but on a slower timescale than the solvent-exposed sites.

The equilibrium molten globule is characterized by a much smaller dispersion in τ. The nonpolar core still displays slower water dynamics than the solvent-exposed sites, consistent with the idea that the MG adopts some of the native-state features. From the DNP and EPR data, we conclude that all the MG core sites studied here directly interact with dynamic water and are therefore "wet".

The U state displays the fastest water dynamics and is characterized by fairly uniform behavior across all sites investigated. The large progressive dispersion in τ, as U turns into MG and then into N, implies that the local protein topology significantly impacts the hydration dynamics landscape.

The role of hydration dynamics in protein folding and other biomolecular processes involving conformational transitions is of active interest. This work shows that the hydration dynamics of apoMb is site-specific and folding-state-dependent. Our DNP results indicate that the investigated core sites of the MG are wet, with hydration dynamics significantly slower than in the U state. Surprisingly, the exterior site E41R1 is hydrated by less dynamic water in the MG than in the N state, suggesting the presence of non-native contacts and highly dynamic side chains in the MG. Consistent with the above observations, the EPR data in the MG showed reduced packing around the core residues and increased conformational heterogeneity for all sites compared to the N state. Thus, the emerging scenario is a conformationally flexible equilibrium MG with a "loose" wet core actively sampling non-native conformations that enable surface residues to become transiently buried. In general, the presence of slowly diffusing hydration water in the MG core may prove to be particularly important in nature. This water may play key roles in protein folding, including, as has been proposed, lubricating or facilitating the conformational sampling necessary to consolidate the loosely packed core side chains into a highly compact (and virtually water-free) N state.[12]

The dramatically different hydration dynamics observed for the different states of apoMb demonstrates that the water within about 10 Å of a protein has distinctly variable properties that are exquisitely sensitive to protein conformation. The dynamics of this hydration water is important in that it is likely to affect thermodynamic stability and interconversion mechanisms among different protein states.

ASSOCIATED CONTENT

Supporting Information. More details of the EPR simulation techniques and results. This material is available free of charge via the Internet at http://pubs.acs.org.

AUTHOR INFORMATION

Corresponding Author

songi@chem.ucsb.edu; cavagnero@chem.wisc.edu

Present Addresses

[‖]Department of Physics, Harvard University, 17 Oxford St., Cambridge, MA 02138

[#]College of Pharmacy, University of Michigan, Ann Arbor, MI 48109

[▽]Department of Biochemistry, University of Wisconsin—Madison, Madison, WI 53706

ACKNOWLEDGMENT

The authors thank Peter E. Wright for helpful discussions and Anna Pavlova for help with sample preparation. S.H. acknowledges funding from the Packard Fellowship for Science and Engineering, the NSF CAREER Award (CHE 0645536) and partial support from the NSF MRSEC (DMR05-20415) supported Materials Research Laboratory (MRL), as well as usage of the MRL Central Facilities—a member of the NSF-funded Materials Research Facilities Network (www.mrfn.org). S.C. was funded by NSF grants MCB-095129 and MCB-0544182, and W.H. received funding from NIH Grant 5R01 EY005216 and the Jules Stein Professor Endowment.

REFERENCES

(1) Kauzmann, W. *Adv. Protein Chem.* **1959**, *14*, 1–63.
(2) Dill, K. A. *Biochemistry* **1990**, *29*, 7133–7155.
(3) Cheung, M. S.; Garcia, A. E.; Onuchic, J. N. *Proc. Natl. Acad. Sci. U.S.A* **2002**, *99*, 685–690.
(4) Dyson, H. J.; Wright, P. E.; Scheraga, H. A. *Proc. Natl. Acad. Sci. U.S.A.* **2006**, *103*, 13057–13061.
(5) Kim, P. S.; Baldwin, R. L. *Annu. Rev. Biochem.* **1982**, *51*, 459–489.
(6) Roder, H.; Colon, W. *Curr. Opin. Struct. Biol.* **1997**, *7*, 15–28.
(7) Kuwajima, K. *Proteins* **1989**, *6*, 87–103.
(8) Ptitsyn, O. B. *Adv. Protein Chem.* **1995**, *47*, 83–229.
(9) Denisov, V. P.; Jonsson, B. H.; Halle, B. *Nat. Struct. Biol.* **1999**, *6*, 253–260.
(10) Jha, S. K.; Udgaonkar, J. B. *Proc. Natl. Acad. Sci. U.S.A.* **2009**, *106*, 12289–12294.
(11) Kamei, T.; Oobatake, M.; Suzuki, M. *Biophys. J.* **2002**, *82*, 418–425.
(12) Sheinerman, F. B.; Brooks, C. L. *Proc. Natl. Acad. Sci. U.S.A.* **1998**, *95*, 1562–1567.
(13) Baldwin, R. L.; Frieden, C.; Rose, G. D. *Proteins: Struct., Funct. Bioinf.* **2010**, *78*, 2725–2737.
(14) Shakhnovich, E. I.; Finkelstein, A. V. *Biopolymers* **1989**, *28*, 1667–1680.
(15) Kramers, H. A. *Physica* **1940**, *7*, 284–304.
(16) Manke, C. W.; Williams, M. C. *Macromolecules* **1985**, *18*, 2045–2051.
(17) Ansari, A.; Jones, C. M.; Henry, E. R.; Hofrichter, J.; Eaton, W. A. *Science* **1992**, *256*, 1796–1798.
(18) Frauenfelder, H.; Chen, G.; Berendzen, J.; Fenimore, P. W.; Jansson, H.; McMahon, B. H.; Stroe, I. R.; Swenson, J.; Young, R. D. *Proc. Natl. Acad. Sci. U.S.A.* **2009**, *106*, 5129–5134.
(19) Frauenfelder, H.; Fenimore, P. W.; McMahon, B. H. *Biophys. Chem.* **2002**, *98*, 35–48.
(20) Jansson, H.; Kargl, F.; Fernandez-Alonso, F.; Swenson, J. *J. Chem. Phys.* **2009**, *130*, 205101–13.
(21) Bhat, T. N.; Bentley, G. A.; Boulot, G.; Greene, M. I.; Tello, D.; Dallacqua, W.; Souchon, H.; Schwarz, F. P.; Mariuzza, R. A.; Poljak, R. J. *Proc. Natl. Acad. Sci. U.S.A.* **1994**, *91*, 1089–1093.
(22) Kurkal, V.; Daniel, R. M.; Finney, J. L.; Tehei, M.; Dunn, R. V.; Smith, J. C. *Chem. Phys.* **2005**, *317*, 267–273.
(23) Halle, B.; Nilsson, L. *J. Phys. Chem. B* **2009**, *113*, 8210–8213.
(24) Johnson, M. E.; Malardier-Jugroot, C.; Murarka, R. K.; Head-Gordon, T. *J. Phys. Chem. B* **2009**, *113*, 4082–4092.
(25) Zhang, L.; Wang, L.; Kao, Y.-T.; Qiu, W.; Yang, Y.; Okobiah, O.; Zhong, D. *Proc. Natl. Acad. Sci. U.S.A.* **2007**, *104*, 18461–18466.
(26) Zhang, L.; Yang, Y.; Kao, Y.-T.; Wang, L.; Zhong, D. *J. Am. Chem. Soc.* **2009**, *131*, 10677–10691.
(27) Rupley, J. A.; Gratton, E.; Careri, G. *Trends Biochem. Sci.* **1983**, *8*, 18–22.
(28) Chandler, D. *Nature* **2005**, *437*, 640–647.
(29) Daidone, I.; Ulmschneider, M. B.; Di Nola, A.; Amadei, A.; Smith, J. C. *Proc. Natl. Acad. Sci. U.S.A.* **2007**, *104*, 15230–15235.
(30) Levy, Y.; Onuchic, J. N. *Annu. Rev. Biophys. Biomed.* **2006**, *35*, 389–415.
(31) Makarov, V. A.; Andrews, B. K.; Smith, P. E.; Pettitt, B. M. *Biophys. J.* **2000**, *79*, 2966–2974.
(32) Russo, D.; Hura, G.; Head-Gordon, T. *Biophys. J.* **2004**, *86*, 1852–1862.
(33) Otting, G.; Liepinsh, E.; Halle, B.; Frey, U. *Nat. Struct. Mol. Biol.* **1997**, *4*, 396–404.
(34) Hodges, M. W.; Cafiso, D. S.; Polnaszek, C. F.; Lester, C. C.; Bryant, R. G. *Biophys. J.* **1997**, *73*, 2575–2579.
(35) Persson, E.; Halle, B. *Proc. Natl. Acad. Sci. U.S.A.* **2008**, *105*, 6266–6271.
(36) Venu, K.; Anders Svensson, L.; Halle, B. *Biophys. J.* **1999**, *77*, 1074–1085.
(37) Qvist, J.; Persson, E.; Mattea, C.; Halle, B. *Faraday Discuss.* **2009**, *141*, 131–144.
(38) Nakagawa, H.; Joti, Y.; Kitao, A.; Kataoka, M. *Biophys. J.* **2008**, *95*, 2916–2923.
(39) Smith, J. C. *Q. Rev. Biophys.* **1991**, *24*, 227–291.
(40) Zanotti, J. M.; Hervé, G.; Bellissent-Funel, M. C. *BBA—Proteins Proteom.* **2006**, *1764*, 1527–1535.
(41) Ebbinghaus, S.; Kim, S. J.; Heyden, M.; Yu, X.; Heugen, U.; Gruebele, M.; Leitner, D. M.; Havenith, M. *Proc. Natl. Acad. Sci. U.S.A.* **2007**, *104*, 20749–20752.
(42) Kim, S. J.; Born, B.; Havenith, M.; Gruebele, M. *Angew. Chem., Int. Ed.* **2008**, *47*, 6486–6489.
(43) Pal, S. K.; Peon, J.; Zewail, A. H. *Proc. Natl. Acad. Sci. U.S.A.* **2002**, *99*, 1763–1768.
(44) Pal, S. K.; Peon, J.; Zewail, A. H. *Proc. Natl. Acad. Sci. U.S.A.* **2002**, *99*, 15297–15302.
(45) Nucci, N. V.; Pometun, M. S.; Wand, A. J. *Nat. Struct. Mol. Biol.* **2011**, *18*, 245–249.
(46) Halle, B. *J. Chem. Phys.* **2003**, *119*, 12372–12385.
(47) Hausser, K. H.; Stehlik, D. *Adv. Magn. Reson.* **1968**, *3*, 79–139.
(48) Armstrong, B. D.; Han, S. *J. Am. Chem. Soc.* **2009**, *131*, 4641–4647.
(49) Hughson, F.; Wright, P.; Baldwin, R. *Science* **1990**, *249*, 1544–1548.
(50) Eliezer, D.; Chung, J.; Dyson, H. J.; Wright, P. E. *Biochemistry* **2000**, *39*, 2894–2901.
(51) Eliezer, D.; Jennings, P. A.; Dyson, H. J.; Wright, P. E. *FEBS Lett.* **1997**, *417*, 92–96.
(52) Eliezer, D.; Wright, P. E. *J. Mol. Biol.* **1996**, *263*, 531–538.
(53) Nishiguchi, S.; Goto, Y.; Takahashi, S. *J. Mol. Biol.* **2007**, *373*, 491–502.
(54) Kuriyan, J.; Wilz, S.; Karplus, M.; Petsko, G. A. *J. Mol. Biol.* **1986**, *192*, 133–154.
(55) López, C. J.; Fleissner, M. R.; Guo, Z.; Kusnetzow, A. K.; Hubbell, W. L. *Protein Sci.* **2009**, *18*, 1637–1652.
(56) Jennings, P. A.; Wright, P. E. *Science* **1993**, *262*, 892–896.
(57) Eliezer, D.; Yao, J.; Dyson, H. J.; Wright, P. E. *Nat. Struct. Mol. Biol.* **1998**, *18*, 148–155.
(58) Nishimura, C.; Dyson, H. J.; Wright, P. E. *Proc. Natl. Acad. Sci. U.S.A.* **2005**, *102*, 4765–4770.
(59) Uzawa, T.; Nishimura, C.; Akiyama, S.; Ishimori, K.; Takahashi, S.; Dyson, H. J.; Wright, P. E. *Proc. Natl. Acad. Sci. U.S.A.* **2008**, *105*, 13859–13864.
(60) Bertagna, A. M.; Barrick, D. *Proc. Natl. Acad. Sci. U.S.A.* **2004**, *101*, 12514–12519.
(61) Chow, C. C.; Chow, C.; Raghunathan, V.; Huppert, T. J.; Kimball, E. B.; Cavagnero, C. *Biochemistry* **2003**, *42*, 7090–7099.
(62) Jennings, P. A.; Stone, M. J.; Wright, P. E. *J. Biomol. NMR* **1995**, *6*, 271–276.
(63) Armstrong, B. D.; Lingwood, M. D.; McCarney, E. R.; Brown, E. R.; Bluemler, P.; Han, S. *J. Magn. Reson.* **2008**, *191*, 273–281.
(64) Armstrong, B. D.; Han, S. *J. Chem. Phys.* **2007**, *127*, 104508–10.
(65) Muller-Warmuth, W.; Meise-Gresch, K. *Adv. Magn. Reson.* **1983**, *11*, 1–45.
(66) Hausser, K. H.; Stehlik, D. *Adv. Magn. Reson.* **1968**, *3*, 79–139.
(67) Freed, J. H. *J. Chem. Phys.* **1978**, *68*, 4034–4037.
(68) Hwang, L.-P.; Freed, J. H. *J. Chem. Phys.* **1975**, *63*, 4017–4025.
(69) Hofer, P.; Parigi, G.; Luchinat, C.; Carl, P.; Guthausen, G.; Reese, M.; Carlomagno, T.; Griesinger, C.; Bennati, M. *J. Am. Chem. Soc.* **2008**, *130*, 3254–3255.
(70) Polnaszek, C. F.; Bryant, R. G. *J. Chem. Phys.* **1984**, *81*, 4038–4045.
(71) Bennati, M.; Luchinat, C.; Parigi, G.; Turke, M.-T. *Phys. Chem. Chem. Phys.* **2010**, *12*, 5902–5910.
(72) Sezer, D.; Gafurov, M.; Prandolini, M. J.; Denysenkov, V. P.; Prisner, T. F. *Phys. Chem. Chem. Phys.* **2009**, *11*, 6638–6653.
(73) Sezer, D.; Prandolini, M. J.; Prisner, T. F. *Phys. Chem. Chem. Phys.* **2009**, *11*, 6626–6637.

(74) Guo, Z.; Cascio, D.; Hideg, K.; Kálái, T.; Hubbell, W. L. *Protein Sci.* **2007**, *16*, 1069–1086.
(75) Baldwin, E.; Xu, J.; Hajiseyedjavadi, O.; Baase, W. A.; Matthews, B. W. *J. Mol. Biol.* **1996**, *259*, 542–559.
(76) Anderson, D. E.; Hurley, J. H.; Nicholson, H.; Baase, W. A.; Matthews, B. W. *Protein Sci.* **1993**, *2*, 1285–1290.
(77) Richards, F. M.; Wynn, R.; Harkins, P. C.; Fox, R. O. *Protein Sci.* **1997**, *6*, 1621–1626.
(78) Wynn, R.; Harkins, P. C.; Richards, F. M.; Fox, R. O. *Protein Sci.* **1996**, *5*, 1026–1031.
(79) Olson, J. S.; Soman, J.; Phillips, G. N. *IUBMB Life* **2007**, *59*, 552–562.
(80) Armstrong, B. D.; Soto, P.; Shea, J.-E.; Han, S. *J. Magn. Reson.* **2009**, *200*, 137–141.
(81) Kausik, R.; Han, S. *J. Am. Chem. Soc.* **2009**, *131*, 18254–18256.
(82) Griffith, O. H.; Dehlinger, P. J.; Van, S. P. *J. Membr. Biol.* **1974**, *15*, 159–192.
(83) Marsh, D. *Proc. Natl. Acad. Sci. U.S.A.* **2001**, *98*, 7777–7782.
(84) Owenius, R.; Engstrom, M.; Lindgren, M.; Huber, M. *J. Phys. Chem. A* **2001**, *105*, 10967–10977.
(85) Kiihne, S.; Bryant, R. G. *Biophys. J.* **2000**, *78*, 2163–2169.
(86) Lecomte, J. T. J.; Kao, Y. H.; Cocco, M. J. *Proteins* **1996**, *25*, 267–285.
(87) Value for free Tempo is taken from ref 47. As noted in the Materials and Methods section, there are more recent reports on the coupling factor with different values.[6870−72] The data on apoMb presented here were taken with the same experimental setup and conditions as ref 47, and are therefore the relevant number for this comparison.
(88) Columbus, L.; Kalai, T.; Jeko, J.; Hideg, K.; Hubbell, W. L. *Biochemistry* **2001**, *40*, 3828–3846.
(89) McHaourab, H. S.; Lietzow, M. A.; Hideg, K.; Hubbell, W. L. *Biochemistry* **1996**, *35*, 7692–7704.
(90) Gardino, A. K.; Villali, J.; Kivenson, A.; Lei, M.; Liu, C. F.; Steindel, P.; Eisenmesser, E. Z.; Labeikovsky, W.; Wolf-Watz, M.; Clarkson, M. W.; Kern, D. *Cell* **2009**, *139*, 1109–1118.
(91) Fraser, J. S.; Clarkson, M. W.; Degnan, S. C.; Erion, R.; Kern, D.; Alber, T. *Nature* **2009**, *462*, 669–673.
(92) Yao, J.; Chung, J.; Eliezer, D.; Wright, P. E.; Dyson, H. J. *Biochemistry* **2001**, *40*, 3561–3571.